

LAMINAR FLOW WING'S OPTIMIZATION DESIGN BY RANS SOLVER WITH AUTOMATIC TRANSITION PREDICTION

Song Wenping*, Zhu Zhen*, Yang Hui*, Zhang Kun*, Liu Jun*

*National Key Laboratory of Aerodynamic Design and Research, Northwestern Polytechnical University, Xi'an 710072, P. R. China

wpsong@nwpu.edu.cn

Keywords: transition prediction, e^N method, RANS solver, Kriging model, optimization

Abstract

A high fidelity RANS Solver coupling the reliable transition prediction model and a practical optimizer with high efficiency and reliability are two key issues in the design of the natural laminar flow wings. This paper aims at developing a practical tool for the laminar flow wing's optimization design by combining the above mentioned two issues.

Firstly, a N_{TS}/N_{CF} transition prediction method based on the linear stability theory is coupled to the in-house three-dimensional RANS solver for improving the simulation precision of the solver. By solving the three dimensional linear stability equations, the N_{TS} which corresponds to the Tollmien-Schlichting instability is integrated with the envelope strategy, and the N_{CF} which corresponds to the crossflow instability is integrated with the fixed β strategy.

With the transition N factors N_{TS} and N_{CF} being determined according to the experimental data, a Reynolds-Averaged Navier-Stokes solver with the functionality of automatic laminar-turbulent transition prediction is developed.

Secondly, combined with the optimization method based on the Kriging surrogate model and the genetic algorithm, an optimization method for the laminar flow wings' optimization design is developed.

Finally, with the developed method, the drag minimization of a baseline natural laminar flow (NLF) wing by changing the wing planform with the constraints of wing's area keeping nearly constant and lift being not decreased is studied. The results show that the drag coefficient is

decreased by 4.47%, and the area of laminar flow on the wing surface is enlarged. This shows that the method in this paper can be effectively applied to the aerodynamic design of natural laminar flow wing.

1 Introduction

In order to improve the performance of the aircraft and to reduce the fuel consumption & CO₂ emission during the cruise, the cruise drag needs to be further reduced. In general, for a typical swept-winged transport aircraft at cruise, the frictional drag accounts for about 35% of the total drag [1], so among the various drag reduction technologies, through maintaining extended natural laminar flow on the surface of aircraft to reduce frictional drag is one of the most promising technologies. For this reason, the natural laminar flow wing's design is considered as one of the key technologies to improve the performance of the next generation of aircrafts. However, the design of natural laminar flow wing on which a wide range of laminar flow can be maintained must be based on the reliable laminar-turbulent transition prediction method. Although we still cannot make a complete explanation of the transition mechanism yet because of its complexity, after half a century's theoretical and experimental research, there has been quite in-depth understanding of the transition mechanism and a lot of methods for predicting the boundary layer transition have been developed. Among those methods, the e^N method proposed by Smith, Gamberoni [2] and Van Ingen [3], which based

on the linear stability theory(LST), is most popular and has been widely used in industrial design applications. In view of the e^N method having been successfully applied in two-dimensional boundary layer transition prediction, Malik [4], Mack [5], Arnal [6], Cebeci [7] and other investigators introduced this method into determining the three-dimensional boundary layer's transition. Especially during the past decade, the German Aerospace Center (also called DLR), the French Aerospace Lab(also called ONERA) and the other research institutes have been focusing on research of coupling the transition prediction criteria to the three-dimensional RANS solver in order to increase the calculation accuracy. Krumbein [8][9] coupled the e^N -database method into a RANS solver to improve the simulation precision of the wing configurations and the three-dimensional high-lift configurations. For the same purpose, Perraud [10] inserted a simplified transition tool into the RANS solver. The transition prediction criteria which were used are simplified e^N method and analytical criteria based on the empirical correlations.

In this paper, as a continued research of [10], we couple an e^N method which is called N_{TS}/N_{CF} transition prediction method to the three-dimensional RANS solver to increase the in-house RANS solver's accuracy. The N_{TS}/N_{CF} transition prediction method needs to compute two N factors, one for Tollmien-Schlichting (TS) disturbances in streamwise velocity profile (the so called N_{TS}), and another for crossflow(CF) disturbances in cross-flow velocity profile (the so called N_{CF}). Transition is assumed to occur for particular combinations of these two N factors. Here, the two N factors do not come from the simplified method or the empirical correlations. They are calculated by solving the three-dimensional linear stability equations using the Cebeci-Stewartson(CS) eigenvalue formulation [7] which is described briefly in section 2. The method of coupling the RANS solver with the transition prediction criterion and the validation of the developed RANS solver with automatic transition prediction are also given in section 2.

On the other hand, the optimization method based on CFD codes has gained more and more applications in aerodynamic design problems. In order to retain the advantage of global optimization methods such as genetic algorithm and reduce the computational cost of time-consuming CFD codes at the same time, a surrogate-based optimization optimizer [11][12][13] is used in present paper in the drag reduction optimization design of natural laminar wing. In section 3, the Kriging-based surrogate method is described briefly. In section 4, the example of drag reduction optimization by present method is given, and the results show the effectiveness of the developed method.

2 RANS Solver with Automatic Transition Prediction

In order to develop a three dimensional RANS solver with the functionality of automatic transition prediction, we integrated three solvers, a 3-D RANS solver, a 3-D laminar boundary layer solver, a transition prediction solver based on LST and full e^N method, in iterative form. The solution method of three solvers and the iteration process will be described briefly in the following sub-sections.

2.1 Three-dimensional RANS solver

The three dimensional, unsteady, compressible RANS equations in our solver [14] are solved by means of a finite volume approach using a LU-SGS time-stepping method with multi-grid acceleration, and the Spalart-Allmaras (SA) turbulence model is applied. In boundary-layer theory, the pressure gradient is nearly zero along the wall normal direction inside the boundary-layer region. For this reason, the wall pressure distribution from RANS solutions is used as the outer boundary condition for the boundary-layer solution.

2.2 Three-dimensional laminar boundary layer solver

As we all know that the prediction of transition in the flows around wings with the e^N

method requires the specification of velocity and temperature profiles of the laminar boundary layers. Generally there are two ways to obtain the velocity and temperature profiles, either by the direct solutions of the RANS Equation with fixed transition point as far as possible along chord line or by the solutions of the boundary-layer equations. In our paper, we use the latter method to get the velocity and temperature profiles because the former method need very dense grid points in the region of boundary layer to obtain accurate viscous-layer results which will cost huge compute time [15]. In order to solve the boundary-layer on arbitrary wings, we utilize a non-orthogonal coordinate system for defining the wings. Keller's box method is used to discrete the three-dimensional laminar boundary-layer equations, and then, using the Newton method to linearize the nonlinear boundary layer equations. Finally, the Block- Elimination method is used to solve the linear system.

2.3 Transition Prediction Solver

Unlike the simplified e^N method, such as the e^N - database method which does not need to solve the linear stability equation for detecting the transition location, the present method uses the CS eigenvalue formulation to solve the Orr-Sommerfeld equations for three-dimensional flows with spatial theory.

The small disturbance of any fluctuating quantities based on the spatial theory is expressed by

$$\begin{aligned} q' &= \hat{q}(y)e^{i(\alpha x + \beta z - \omega t)} \\ &= \hat{q}(y)e^{-i\alpha_i x - \beta_i z} e^{i(\alpha_r x + \beta_r z - \omega t)} \end{aligned} \quad (1)$$

where, ω is real, α and β are complex: $\alpha = \alpha_r + i\alpha_i$, $\beta = \beta_r + i\beta_i$.

The procedure through using the e^N method to determine the three dimensional boundary layer flows' transition points contains two steps. The first step is to calculate the neutral curve for determining which disturbance will lead to laminar flow transition. The second step is to calculate the amplification rate for different dimensional frequencies beginning from the lower branch of the neutral curve. In this step,

different strategies used for computation of the amplification factor N will generate different e^N methods.

2.3.1. Calculation the N factor with the envelop strategy (Envelop Method)[9]

In the solution of three-dimensional linear stability equations, a relationship between the two complex numbers α and β is required. In the CS eigenvalue formulation the relationship is computed by making use of concepts based on group velocity using the saddle-point discussed by Cebeci and Stewartson. According to the saddle point method the formulation $(\partial\alpha/\partial\beta)_{\omega, Re}$ is real and related by the disturbance angle ϕ through

$$\left(\frac{\partial\alpha}{\partial\beta} \right)_{\omega, Re} = -\tan\phi \quad (2)$$

The Eq. (2) provides a relationship between the two wave numbers which are needed in the eigenvalue problem.

In the first step, the absolute neutral curve, which was named as "zarf" by Cebeci, is calculated with the additional condition provided by the Eq. (2). The zarf passes through the critical points in $\alpha, \beta, \omega, Re$ space at which $Re = Re_{cr}$, here Re is the chord Reynolds number. In the second step, the amplification rate for different dimensional frequencies beginning from the lower branch of the zarf is calculated. The amplification rate Γ is:

$$\Gamma = -\alpha_i + \beta_i \left(\frac{\partial\alpha}{\partial\beta} \right)_{\omega, Re} \quad (3)$$

The onset of transition may be evaluated by solving the integral

$$N = \max_f \left[\int_{x_0}^x \max_{\phi} \Gamma dx \right] \quad (4)$$

where f is the dimensional frequency $\omega^*/2\pi$, ω^* is the dimensional radian frequency, x_0 corresponds to the x -location where the amplification rate is zero on the zarf. Once the amplification factor N is greater than a limiting factor N_{tr} , then the transition happens.

From our study, by comparison with existing experimental data, we found that the N factors calculated by this method can give a reliable threshold $(N_{TS})_{tr}$ for TS induced transition.

2.3.2. Calculation the N factor with the fixed β strategy (Fixed β Method)

In this strategy the N factor is calculated by maximizing the total amplification with respect to both f and β_r . The onset of transition may be evaluated by solving the integral

$$N = \max_f \left[\max_{\beta_r} \int_{x_0}^x \Gamma dx \right] \quad (5)$$

here, in the first step of the transition procedure, we still use the CS eigenvalue formulation to get the “zarf” for determining the unstable disturbance’s frequencies f . For the sake of simplicity, we assume that $\beta_i=0$. Then, a series of β_r which may cause the boundary layer flow transition can be determined on a natural curve with a fixed frequency f .

As many combinations of f and β need to be considered, it requires more computational effort. In this paper, we just calculate the N factors which correspond to $f=0$ Hz. The cross-flow wave with $f=0$ Hz is called stationary wave which is considered the main reason for the three dimensional boundary layer’s transition.

By comparison with existing experimental data, we found that this method can give a reliable threshold $(N_{CF})_{tr}$ for the crossflow induced transition.

2.3.3. Transition prediction with the N_{TS}/N_{CF} method

Since it is unknown that for a realistic problem the transition is caused by TS instability or CF instability, we developed the N_{TS}/N_{CF} method combined the Envelop method and Fixed β method. This method explicitly separates TS and CF disturbances. This method uses two threshold factors $(N_{TS})_{tr}$ and $(N_{CF})_{tr}$ to detect the transition point. For a given problem, we calculate the N_{TS} and N_{CF} along the streamwise using Eq.(4) and Eq.(5) respectively. Once, any one of the two N factors reaches their

threshold value, and then the transition happens. If the N_{TS} first reaches the $(N_{TS})_{tr}$, the breakdown to turbulence is induced by the TS waves. If the N_{CF} first reaches the $(N_{CF})_{tr}$, the breakdown is induced by the CF waves.

2.4 Calculation procedures

A RANS solver, a laminar boundary solver and a full e^N prediction transition method are coupled (see Fig. 1). First, the flow simulation begins with fixed transition model by the RANS solver. The transition points are fixed near the trailing edge firstly in order to supply the laminar parameters for solving the laminar boundary layer equations. As soon as the steady flow is established, the surface pressure coefficient c_p of the wing is calculated by the RANS solver for determining the outer boundary condition of the laminar boundary layer. Second, after the laminar boundary layer’s outer boundary condition is calculated, the three-dimensional laminar boundary layer equations can be solved. Then, we use the linear stability code to analyze the laminar boundary’s velocity and temperature profiles applied by the boundary layer solver, and find out the transition point with above mentioned method. If the transition position is not found before the boundary layer separation, then, we set the laminar separation point as the transition position approximately. Finally, we returned the transition information to the RANS solver. Repeat the above process, the flow transition point was detected automatically during the ongoing RANS computation.

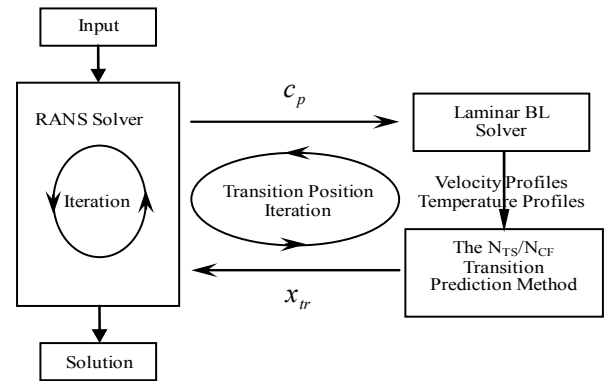


Fig.1 Sketch of the coupling the RANS solver with the transition prediction method

2.5 Validation

The test case is a finite swept wing with the R.A.E.101 airfoil as the sections normal to the leading edge.

The finite swept wing with the 12% thick R.A.E.101 airfoil was tested in the 13ft × 19ft low speed wind tunnel at R.A.E., Bedford [16]. The finite swept wing was a constant chord wing of aspect ratio 5.0, 45° sweep, as shown in Fig.2. The tested wind speed was 200ft/sec and the Reynolds number based on the wing chord was 2.1×10^6 . The C-H structured grid used for calculating is shown in Fig.3. The grid size is $233 \times 105 \times 49$.

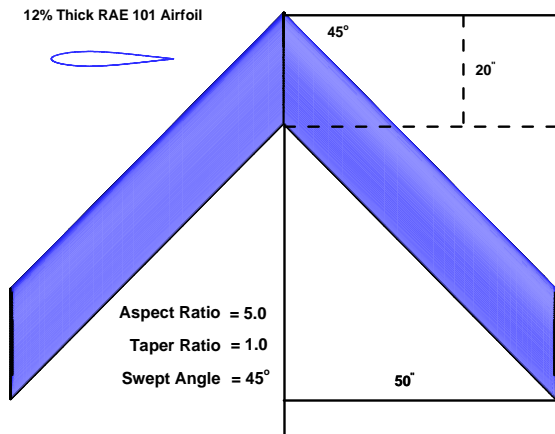


Fig.2 Sketch of the finite swept wing configuration

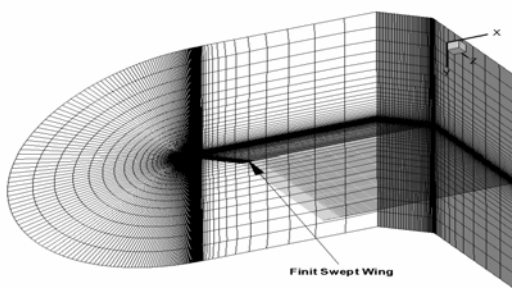


Fig.3 “C-H” type grid for simulating the flow around the finite swept wing by RNAS solver

Fig.4 shows the measured and calculated drag polar of the finite swept wing model. It is obvious that the accuracy of drag coefficients computed by the RANS solver with transition prediction improved greatly compared to the full turbulence RANS solver. Fig.5 gives the comparison of lift to drag ratio which show the same improvement.

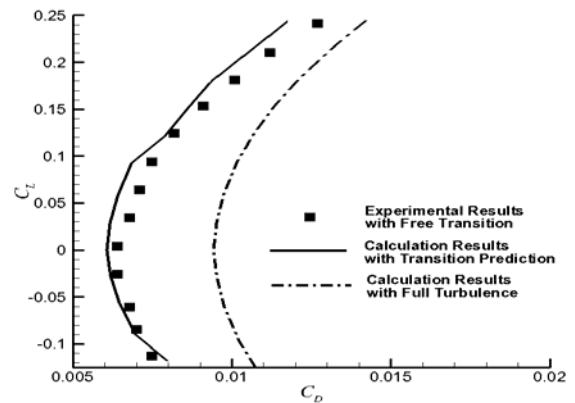


Fig.4 Measured and computed drag coefficients of the finite swept wing with a swept angle $\lambda = 45^\circ$

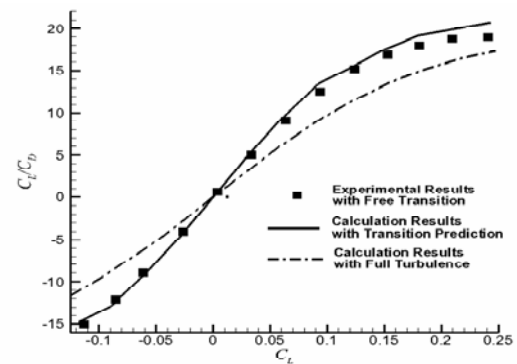


Fig.5 Measured and computed lift to drag ratios of the finite swept wing with a swept angle $\lambda = 45^\circ$

3 Kriging-based optimization system

3.1 Kriging model

Kriging is a statistical interpolation method suggested by Krige [17] in 1951 and mathematically formulated by Matheron [18] in 1963. In 1989, Kriging was extended by Sacks et al [19] for the design and analysis of deterministic computer experiments. Then it was widely used as a surrogate modeling technique for predicting the output of computer codes in simulation-based analysis and optimization [20][21].

3.1.1 Kriging Predictor and Mean Squared Error

The Kriging treats the output of a deterministic computer experiment as a constant term plus a stochastic process:

$$Y(\mathbf{x}) = \beta + Z(\mathbf{x}) \quad (6)$$

The stationary random process $Z(\bullet)$ has mean value of zero and covariance of

$$\text{Cov}[Z(\mathbf{x}), Z(\mathbf{x}')] = \sigma^2 R(\mathbf{x}, \mathbf{x}') \quad (7)$$

where σ^2 is the process variance of $Z(\bullet)$ (it is assumed that $\sigma^2(\mathbf{x}) \equiv \sigma^2$ for all \mathbf{x}), and R is the spatial correlation function that only depends on the Euclidean distance between two sites \mathbf{x} and \mathbf{x}' .

We assume that the output of a computer code can be approximated by a linear combination of the observed data \mathbf{y}_s , the Kriging approximation of $y(\mathbf{x})$ at an untried \mathbf{x} is formally defined as

$$\hat{y}(\mathbf{x}) = \sum_{i=1}^{n_s} w_i y_i = \mathbf{w}^T \mathbf{y}_s \quad (8)$$

where $\mathbf{w} = (w^{(1)}, \dots, w^{(n_s)})^T$ are the weight coefficients (called Kriging weights). We replace $\mathbf{y}_s = (y^{(1)}, \dots, y^{(n_s)})^T$ with the corresponding random quantities $\mathbf{Y}_s = (Y^{(1)}, \dots, Y^{(n_s)})^T$.

By minimizing the Mean Squared Error (MSE) of this predictor, we can obtain the following Kriging predictor

$$\hat{y}(\mathbf{x}) = \hat{\boldsymbol{\beta}} + \mathbf{r}^T(\mathbf{x}) \mathbf{R}^{-1} (\mathbf{y}_s - \mathbf{1} \hat{\boldsymbol{\beta}}) \quad (9)$$

where $\mathbf{1}$ is unit column vector filled with ones and

$$\hat{\boldsymbol{\beta}} = (\mathbf{1}^T \mathbf{R}^{-1} \mathbf{1})^{-1} \mathbf{1}^T \mathbf{R}^{-1} \mathbf{y}_s \quad (10)$$

and

$$\mathbf{R} := [R(\mathbf{x}^{(i)}, \mathbf{x}^{(j)})]_{ij} \in \mathbb{R}^{n_s \times n_s}, \mathbf{r}(\mathbf{x}) := [R(\mathbf{x}^{(i)}, \mathbf{x})]_i \in \mathbb{R}^{n_s}. \quad (11)$$

The MSE of the Kriging prediction at any untried \mathbf{x} can be proven to be

$$\text{MSE}[\hat{y}(\mathbf{x})] = \hat{\sigma}^2 [1 - \mathbf{r}^T \mathbf{R}^{-1} \mathbf{r} + (1 - \mathbf{1}^T \mathbf{R}^{-1} \mathbf{r})^2 / \mathbf{1}^T \mathbf{R} \mathbf{1}] \quad (12)$$

where

$$\hat{\sigma}^2 = \frac{1}{n_s} (\mathbf{y}_s - \mathbf{1} \hat{\boldsymbol{\beta}})^T \mathbf{R}^{-1} (\mathbf{y}_s - \mathbf{1} \hat{\boldsymbol{\beta}}). \quad (13)$$

3.1.2 Correlation Models

The construction of the correlation matrix \mathbf{R} and the correlation vector \mathbf{r} requires the calculation of the correlation functions. The correlation function for random variables at two sites $\mathbf{x}^{(i)}, \mathbf{x}^{(j)}$ is assumed to be only dependent on the spatial distance. Here we focus on a family of correlation models that are of the form

$$R(\mathbf{x}^{(i)}, \mathbf{x}^{(j)}) = \prod_{k=1}^{n_v} R_k(\theta_k, \mathbf{x}_k^{(i)} - \mathbf{x}_k^{(j)}) \quad (14)$$

The correlation function used here is the cubic spline:

$$R_k = \begin{cases} 1 - 15\xi_k^2 + 30\xi_k^3 & \text{for } 0 \leq \xi_k \leq 0.2 \\ 1.25(1 - \xi_k)^3 & \text{for } 0.2 < \xi_k < 1 \\ 0 & \text{for } \xi_k \geq 1 \end{cases}, \text{ where } \xi_k = \theta_k |\mathbf{x}_k^{(i)} - \mathbf{x}_k^{(j)}|. \quad (15)$$

3.1.3 Kriging Fit

Hyper parameters of Kriging $\boldsymbol{\theta} = (\theta_1, \dots, \theta_{n_v})$, can be tuned by solving Maximum Likelihood Estimation (MLE) problem:

$$\text{MLE} = \arg_{\boldsymbol{\theta}} \max \left(-\frac{1}{2} [n_s \ln(\hat{\sigma}^2) + \ln |\mathbf{R}|] \right) \quad (16)$$

3.2 Sampling refinement criteria

After the surrogate model is constructed, the global optimum cannot be found, since the model is not accurate. Additional points should be infilled both to increase the accuracy of the model and to explore the design space. In this paper, two infill strategies are used simultaneously.

3.2.1 Constrained Expected Improvement (EI_c) [13][22]

Expected improvement is defined as the improvement we expect to achieve at an untried site \mathbf{x} . The expected improvement is given by

$$EI[\mathbf{x}] = \begin{cases} (y_{\min} - \hat{y}(\mathbf{x})) \Phi\left(\frac{y_{\min} - \hat{y}(\mathbf{x})}{s(\mathbf{x})}\right) + s(\mathbf{x}) \phi\left(\frac{y_{\min} - \hat{y}(\mathbf{x})}{s(\mathbf{x})}\right) & \text{if } s > 0 \\ 0 & \text{if } s = 0 \end{cases} \quad (17)$$

where $\Phi(\cdot)$ and $\phi(\cdot)$ are the cumulative distribution function and probability density function of standard normal distribution, respectively. s is the root of mean squared error, y_{\min} is the current best objective function value.

Assume we have a constraint $g(\mathbf{x}) > g_{\min}$, the probability that the constraint is fulfilled is as following:

$$P[G > g_{\min}] = \Phi\left(\frac{g_{\min} - \hat{g}(\mathbf{x})}{s(\mathbf{x})}\right) \quad (18)$$

where s is the root of mean squared error of the Kriging Model for the constraint. Then, the constrained expected improvement is:

$$E_c[I(\mathbf{x})] = E[I(\mathbf{x}) \cap G > g_{\min}] = E[I(\mathbf{x})] \cdot P[G > g_{\min}] \quad (19)$$

For multiple constraints, the constrained expected improvement is obtained by multiplying each probability that the constraints fulfilled.

3.2.2 Minimizing the Predictor (MP)

This criterion assumes that the surrogate model is globally accurate and we only need to validate the optimum of the surrogate. The optimum point on the surrogate is found and observed to refine the Kriging model.

3.3 Flowchart of the Kriging-based Optimizer

The flowchart of the developed in-house Kriging-based optimizer is shown in Fig.6. The method of design of experiments for space filling used in this paper is Latin hypercube sampling (LHS), which is one of the most popular modern DOE methods that has found wide application in computational applications [23]. Latin hypercube sampling has the advantage of providing a more accurate estimate of the mean value and can be configured with any numbers of samples and is not restricted to sample size that are specific multiples or powers of dimensionality, besides, it is easy to be coded and cheap to run on computers.

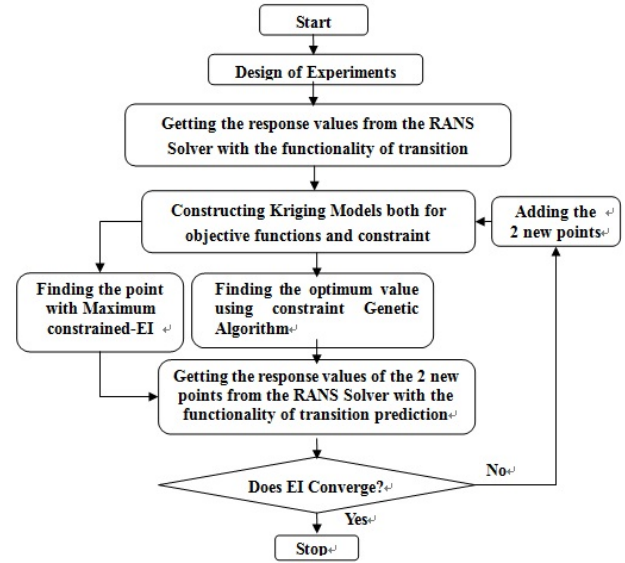


Fig.6 Flowchart of the Kriging-based Optimizer

4 Drag Minimization of NLF Wing

The drag minimization of a NLF wing planform is taken as an example to validate the present method. The chord length of the wing root, the aspect ratio, the taper ratio and the sweep angle of leading edge, are chosen as the four design variables. The geometric constraint is the area of the planform keeping nearly constant. The untwisted baseline wing is chosen as follows:

Root chord : $c=1.0$

Aspect ratio: $\Lambda=8.35$

Taper ratio: $\eta=0.278$

Sweep angle of leading edge: $\chi=16.69^\circ$

Streamwise airfoil section: NLF(1)-0416

The mathematical model of this optimization problem is:

Design point : $Ma=0.69, \alpha=-1.605^\circ, Re=11.7 \times 10^6$

Objective : Minimize: C_D

s.t.:

Aerodynamic constraints : (1) $C_L \geq C_{L0}$

$$(2) |C_m - C_{m0}| / |C_{m0}| \leq 0.05 \quad (20)$$

Geometric constraint: $|A - A_0| / A_0 \leq 0.05$

(A is the projected area of wing)

With the initial 40 sample points evaluated by the developed RANS solver with transition prediction, the optimization is carried out by the process described in Fig.6. Figure 7 gives the

planform of the baseline NLF wing (black line) and the optimized wing (blue line). We can see that the optimized wing has smaller leading edge sweep angle and bigger aspect ratio than the baseline wing, and these changes in the planform of the wing make wider laminar flow region on the wing which can decrease the viscous friction drag. Table 3.1 gives the quantitative comparison of the planform parameters of the baseline wing and the optimized wing. Table 3.2 gives the lift coefficient, drag coefficient, lift to drag coefficient, moment coefficient and laminar flow region coefficient ($S_{laminar}/S_{wing}$) of the baseline wing and the optimized wing. After the optimization design, the drag coefficient is decreased from 0.008637 to 0.008251, i.e. decreased by 4.47%, and the laminar flow surface coefficient is increased from 31.46% to 41.32%.

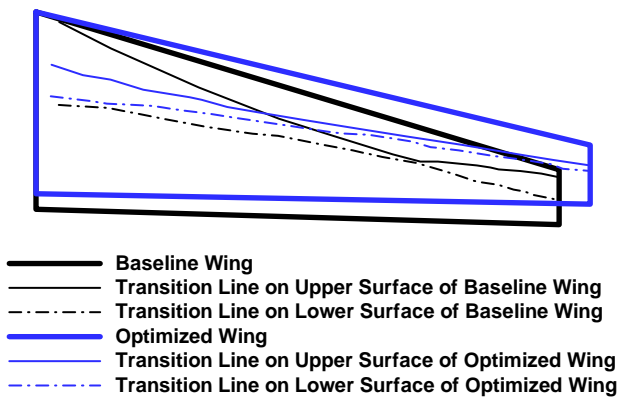


Fig.7 Planforms of the baseline and the optimized wing
(Ma=0.69, Re=11.7E6, $\alpha=-1.605^\circ$)

Table 3.1 Quantitative comparison of the planform parameters of the baseline wing and optimized wing

Parameters	Baseline Wing	Optimized Wing
c	1.0	0.9217
Λ	8.35	9.25
χ	16.69°	13.47°
η	0.278	0.3203

Table 3.2 Optimization results of Kriging model

Parameters	Baseline Wing (RANS Solver)	Optimum Wing (RANS Solver)	Changes
C_L	0.26	0.28254	8.68%
C_D	0.008637	0.008251	-4.47%
C_M	-0.2361	-0.2249	-4.76%
C_L/C_D	30.10	34.24	13.75%
$S_{laminar}/S_{wing}$	31.46%	41.32%	31.34%

The results show that the drag minimization is realized during the optimization process through changing the planform to enlarge the laminar flow range on the wing surface.

5 Conclusion

A drag minimization of a NLF wing considering the planform shape modification is studied in this paper. The results show that the RANS solver with the functionality of predicting the laminar-turbulent transition automatically developed in this paper can be effectively applied to the aerodynamic design of natural laminar flow wing.

Further study will concern on the natural laminar flow wing optimization design that considering the wing section shape modification and planform/section shape modification synchronously.

References

- [1] John E. G. Laminar flow control – back to the future? *AIAA Paper* 2008-3738(2008).
- [2] Smith, A. M. O., and Gamberoni, N. Transition, pressure gradient and stability theory, *Douglas Aircraft Co., Rept.* ES 26388, Long Beach, CA (1956).
- [3] Ingen, J. L. V. A suggested semi-empirical method for the calculation of the boundary layer transition region, *Dept. of Aerospace Engineering, Rept. VTH-74*, Univ. of Delft, Delft, the Netherlands (1956).
- [4] Malik, M. R. COSAL – a black box compressible stability analysis code for transition prediction in three-dimensional boundary layers, *NASA CR - 165925*(1982).
- [5] Mack, L. M. Stability of three-dimensional boundary layers on swept wings at transonic speeds, *IUTAM Symposium, Transsonicum III*, Göttingen(1988).
- [6] Arnal, D., Casalis, G., and Juillen, J. C. Experimental and theoretical analysis of natural transition on infinite swept wing, *IUTAM Symposium*, Toulouse, France, *Laminar-Turbulent Transition* (eds. D. Arnal, R. Michnel) Springer-Verlag, Pp 311-326(1989).
- [7] Cebeci, T. and Stewartson, K. On stability and transition in three-dimensional flows, *AIAA Journal* 18(4): 398-405 (1980).
- [8] Krumbein, A. Automatic transition prediction and application to 3D wing configurations, *AIAA Paper* 2006-914(2006).

- [9] Krumbein, A. Automatic transition prediction and application to 3D high lift configurations, *AIAA Paper* 2006-3164(2006).
- [10] Zhang, K., Song, W. P. Infinite swept-wing reynolds averaged Navier-Stokes computations with full e^N transition criterion, *27th International Congress of the Aeronautical Sciences*, 19-24 Sept.,2010, Nice, France.
- [11] Han, Z. H, Zhang, K. S. Surrogate based optimization, Intec Book, *Real-world Application of Genetic Algorithm*, 2012, pp.343-362
- [12] Song, W. P., Xu, R. F., and Han, Z. H. Study on the improved kriging-based optimization design method, *27th International Congress of the Aeronautical Sciences*, 19-24 Sept.,2010, Nice, France.
- [13] Liu, J., Han, Z. H., and Song, W. P. Efficient kriging-based aerodynamic design of transonic airfoils: some key issues, *50th AIAA Aerospace Sciences Meeting Including the New Horizons Forum and Aerospace Exposition*, 09-12 January 2012, Nashville, Tennessee, AIAA 2012-0967.
- [14] Han, Z. H., He, F., Song, W. P., Qiao Z. D., A preconditioned multigrid method for efficient simulation of three-dimensional compressible and incompressible flows, *Chinese Journal of Aeronautics*, Vol.20, No.4, 2007.
- [15] Stock, H. W., and W. Haase. Feasibility study of e^N transition prediction in Navier–Stokes methods for airfoils, *AIAA Journal* 37(10):1187-1196(1999).
- [16] Brebner, G. G., and L. A. Wyatt. Boundary layer measurements at low speed on two wings of 45° and 55° sweep, *Ministry of Aviation Aeronautical Research Council Current Papers*, C.P. No.554 (1961).
- [17] Krige, D. G. A statistical approach to some basic mine valuations problems on the Witwatersrand, *Journal of the Chemical, Metallurgical and Mining Engineering Society of South Africa*, Vol. 52, No. 6, 1951, pp. 119-139.
- [18] Matheron, G. M. Principles of geostatistics, *Economic Geology*, Vol. 58, No. 8, 1963, pp. 1246-1266.
- [19] Sacks, J., Welch, W. J., Mitchell, T. J., and Wynn, H. P.. Design and analysis of computer experiments, *Statistical Science*, Vol. 4,1989, pp. 409-423.
- [20] Han, Z.-H., Goertz, S., and Zimmermann, R., Improving variable-fidelity surrogate modeling via gradient-enhanced kriging and a generalized hybrid bridge function, *Aerospace Science and Technology*, Jan. 2012. doi:10.1016/j.ast.2012.01.006.
- [21] Han, Z.-H., Zimmermann, R., and Görtz, S., Alternative cokriging model for variable-fidelity surrogate modeling, *AIAA Journal*, Vol. 50, No. 5, 2012, pp.1205-1210. doi: 10.2514/1.J051243
- [22] Forrester, A. I. J. and Keane, A. J. Recent advances in surrogate-based optimization, *Progress in Aerospace Sciences*, Vol. 45, 2009.
- [23] Anthony A. Giunta, Steven F. Wojtkiewicz Jr., and Michael S. Eldred, Overview of modern design of

experiments for computational simulations, *41st Aerospace Sciences Meeting and Exhibit*, 6-9 January 2003, Reno, Nevada, AIAA 2003-649.

6 Acknowledgments

The research is partly funded by the Chinese Aviation Science Funds (2009ZA53008).

Copyright Statement

The authors confirm that they, and/or their company or organization, hold copyright on all of the original material included in this paper. The authors also confirm that they have obtained permission, from the copyright holder of any third party material included in this paper, to publish it as part of their paper. The authors confirm that they give permission, or have obtained permission from the copyright holder of this paper, for the publication and distribution of this paper as part of the ICAS2012 proceedings or as individual off-prints from the proceedings.